Journal of Materials Chemistry B

Accepted Manuscript

ROYAL SOCIETY OF CHEMISTRY

www.rsc.org/materialsB

Smart electroconductive bioactive ceramics to promote *in situ* electrostimulation of bone

Diogo Mata[a*], Filipe J. Oliveira[a], Miguel A. Neto[a], Manuel Belmonte[b], Alexandre C. Bastos[a], Maria A. Lopes[c], Pedro S. Gomes[d], Maria H. Fernandes[d], Rui F. Silva[a]

[a]CICECO, Materials and Ceramic Eng. Dept., Univ. of Aveiro, 3810-193 Aveiro (Portugal)

[b]Institute of Ceramics and Glass, CSIC, 28049 Madrid (Spain)

[c]CEMUC, Metallurgical and Materials Eng. Dept., Faculty of Eng., Univ. of Porto, 4200-465 Porto (Portugal)

[d]Laboratory for Bone Metabolism and Regeneration, Faculty of Dental Medicine, Univ. of Porto, 4200-465 Porto (Portugal)

[*]Corresponding author

Fax: +351 234 425 300
E-mail address: diogomata@ua.pt (D. Mata)

Abstract

Biomaterials can still be reinvented to become simple and universal bone regeneration solutions. Following this roadmap, conductive CNT-based "smart" materials accumulate exciting grafting qualities for tuning the *in vitro* cellular phenotype.

Biphasic electrical stimulation of human osteoblastic cells was performed *in vitro* on either dielectric bioactive bone grafts or conductive CNT-reinforced composites. The efficiency of the electrical stimuli delivering, as well as the effect of the stimulation in the cellular functions were investigated. Conductive substrates boosted the local increase of the culture medium conductivity and the confinement of the exogenous electrical fields. Hence, bone cells proliferation, DNA content and mRNA expression were maximized on conductive substrates yielding superior stimuli delivering efficiency over dielectric ones. These findings are suggestive that bioactive bone grafts with electrical conductivity are able of a high spatial and temporal control of bone cells stimulation.

1. Introduction

Bone regenerative medicine has noticed huge progress in the past decades driven by the great socioeconomic interest in treating skeletal diseases [1]. While there have been tremendous improvements of synthetic bone grafts materials, most are still incapable of fully repair and regenerate severe bone injuries [2]. The development of solutions followed the routes of complex tissue engineering, involving cell manipulation, and of simpler strategies such as "smart" bone grafts with new functionalities, able of stimulating specific phenotype expressions of osteoblastic cells [2, 3]. One such exciting functionality is to take advantage of the piezoelectric effect of bone. The forces exerted internally on the bone generate electrical signals that are carried to the bone cells, thus helping to regulate their biological functions [4, 5]. These electrical currents found in healthy bone are not expected to exist at the fractured bone site, in case of bone tissue damage or loosening. So, it was thought that the use of exogenous electric fields would mimic the mislaid endogenous electric signals and accelerates bone healing [6].

Electrical stimulation, broadly attained by capacitive coupled electrical field, direct current field and electromagnetic field has been used to enhance the bone healing process by activating voltage-gated Ca2+ channels in osteoblast cell plasma membranes [7-9]. In vitro, the direct application of electric current has been found to induce cell elongation, modulate cell alignment, and to favor the migration and invasion of human mesenchymal stem cells (hMSCs) into injured sites [10]. Electrical stimulation also seems to enhance the cell proliferation and the osteogenic differentiation of osteoblastic precursor cells [11, 12]. These findings seem to substantiate the improved musculoskeletal healing attained with electrical stimulation

in clinical trials aiming different applications of bone repair/regeneration, as reviewed in [13-15].

These data have inspired the development of conductive synthetic matrices to assist in the bone regeneration process under electric stimulation [16, 17]. This comes particularly useful since electric/electromagnetic strategies are spatially non-delimited, indiscriminately affecting both target and non-targeting anatomical locations. In the latter, the likely activation of voltage-dependent pathway signals in the surrounding tissues may lead to an overloaded concentration of the internal Ca^{2+} concentration in cells causing functional disorders (e.g. oxidative stress, cytotoxicity) and its premature apoptosis [18, 19]. Ideally for clinical application, the electric stimuli should be confined within the tissue volume expected to be regenerated.

The use of metal containing bone grafts in electrical stimulation protocols is precluded due to corrosion phenomenon that induces cytotoxicity [20]. The characteristics of carbon nanotubes (CNTs), namely the ultimate electrical conductivity in a non-metallic phase and their high aspect-ratio, make them the highest performance filler to obtain highly conductive biomaterials at low percolation thresholds, without damaging the biological profile of the matrix. While several polymeric matrixes [11, 16, 21, 22] and mesoporous silica [23] have been imparted with CNTs to improve their characteristics, these matrices are essentially non bioactive and thus fail to exert an osteoconductive, osteoinductive or ostegenic action within the neighboring bone. Ceramic/glass-based substrates may be able to sustain a bioactive profile in contact with the bone and, in a process mediated by the CNTs enclosure, endure the scaffold material with electrical conductivity. CNTs were used as mechanical reinforcement of dielectric bone grafts, namely HA (hydroxyapatite) reinforced composites, proving that the mechanical properties, bioactivity and osteointegration were improved relatively to single phase HA even if electrical

stimulation was not considered [24, 25]. For electrical functionality to be used, the level of CNT individualization should be enough to allow a low electrical percolation threshold and to improve, or at least avoid, the degradation of the mechanical properties relatively to those of the matrix. The difficulty in doing so means that CNT agglomerates will always be present and that they should be kept within biologically safe diameter sizes (<20 μm) [26]. Their presence insures, nevertheless, that the contact area between CNTs and bone cells will be larger (≈60 μm) and may also give rise to other functionalities. In the bundles there will be cell accessible CNTs that having nano-topography may control cells orientation, migration and also enhance cell adhesion and proliferation [27, 28]. Also, CNTs in the bundles could be provided with functional groups able of anchoring bioactive molecules (e.g. bone morphogenic proteins - BMPs) and drugs (e.g antibiotics) that can be then delivered in situ to the fractured site while simultaneously doing electrical stimulation [29].

It was the main motivation of the work presented here to develop and in-vitro test a CNT/HA/Glass composite material having the adequate mechanical, electrical, microstructural and, most important, biological characteristics, to apply as electroconductive bone graft. The available literature describes the osteoblastic cell response to electrical stimulation either on non-conductive or on conductive substrates. However, comparative studies reporting on the efficiency of stimuli delivering on dielectric and conductive substrates are not found. The use of AC impedance spectroscopy and of vibrating voltage probe measurements in α-MEM (minimal essential medium) reveal the converging effects the conductive composite material have on the electric field and current flow paths. Results for the cell viability/proliferation, DNA content and gene expression increase proved that electrical stimulation clearly induced cell growth and differentiation on the electroconductive bio-composite. The results validate the hypothesis that these new

biodegradable CNT/HA/Glass bone grafts could be used together with a non-invasive electrical stimulation technique to activate cell growth preferentially in the healing zone of the bone.

2. Materials and methods

2.1. Preparation of CNT/Glass/HA samples

Bioglass (65 P_2O5, 15CaO, 10CaF_2, 10Na_2O mol%) and HA powders were lab-prepared from high purity (>98%) grade reagents: the glass was formed at 1450 °C for 90 min in a platinum crucible then rapidly cooled to room temperature; HA was synthesised by a conventional precipitation method.

Commercially available CNTs (NC7000, Nanocyl, Belgium) were used in this work for preparing the composites. The CNTs were purified (>99%) following a non-destructive procedure that involved an annealing at 1900°C for 8h in a flowing Ar atmosphere. CNT/Glass/HA composite powder suspensions were mixed in isopropyl alcohol by a non-destructive process with volume fractions of 4.4 vol% CNTs, above the electric percolation threshold, and densified by hot pressing at fixed pressure of 30 MPa for 60 min at 1100ºC. Full description of these processes was reported previously[30, 31].

2.2. Characterization of samples

Microstructural characterization was carried out on polished surfaces of selected samples by scanning electron microscope, SEM (Hitachi, SU-70). X-ray diffraction (X'PERT-MPD Philips, CuKα1 radiation (λ= 0.154056 nm) with a step size of 0.02º) and Raman spectroscopy (Alpha300 WITec GmbH) were used to identify

the different phases present in the Glass/HA matrix and in the 4.4vol% CNTs composite. Raman imaging was performed using an excitation wavelength of 532 nm. For the imaging, 75 points were acquired per line for a total of 75 lines. The scan size was 80 x 80 μm^2 and 90 ms of acquisition time per spectrum. Mechanical characterization (biaxial flexural and compressive tests) was carried out using a Zwick/Roell Z020 equipment with a load cell of 2.5 kN, under a constant displacement rate of 0.3 and 1 $mm.min^{-1}$, respectively. The biaxial flexural strength values were measured using the circular plate geometry with the 20 mm diameter discs, according to ASTM F394-76: the specimen is supported by 3 ball bearings spaced 120° apart on a 13 mm diameter circle. Loading was applied by a cylinder with a flat loading face with 1.0 mm diameter. For the compressive strength, a cross head speed of 1.0 $mm.min^{-1}$ was used for the 2.5 × 2.5 × 4.5 mm^3 samples. Samples of similar dimensions were used to measure the DC electrical conductivity of the Glass/HA and CNT/Glass/HA materials by fixing copper wires to the smaller faces of the 2.5 x 2.5 x 4.5 mm^3 parallelepipeds. The characterization was performed at room temperature in a Keithley 617 programmable electrometer, with voltage applied in 0.5 V steps in the range of 0-100 V for dielectric samples. For the conductive samples, a programmable power supply (ISO-TECH IPS-603) was used by applying a voltage in the range 0-1 V in 0.1 V steps.

2.3. Electrical field lines in α-MEM solution

In order to evaluate the effect of conductive substrates on the electrical behavior the culture medium used in cell proliferation studies, the resistance of α-Minimal Essential Medium (α-MEM) with different conductive samples (CNT/Glass/HA, highly ordered pyrolytic graphite - HOPG and stainless steel 316L - SS316L) was measured

by electrochemical impedance spectroscopy (EIS) with a Autolab PGstat 302N (Eco Chemie, The Netherlands). A two electrode arrangement was used with spiral platinum electrodes having the solution and the conductive samples between them. The impedance of the electrochemical cell was measured in the 100 kHz to 10 Hz frequency range with 7 points per decade logarithmically distributed; the sinusoidal perturbation was 10 mV rms at open circuit potential (OCP). The effect of different substrate geometry on the current paths was also assessed by measuring the current lines in solution (12 ml α-MEM) using with a vibrating voltage probe, under $3mV.cm^{-1}$ of applied electrical field and of 100 μA of current. The equipment used was manufactured by Applicable Electronics Inc. (USA) and controlled by the ASET 2.0 program developed by Sciencewares (USA). The vibrating microelectrode was a polymer insulated Pt-Ir microwire with a 20 μm diameter platinum black sphere electrodeposited on the tip. The probe vibrates in 2 orthogonal directions (X and Z) and measures the potential difference between the two ends of the vibration. The potential difference divided by the distance between the extremes of vibration gives the local electric field which can be converted to a local current density by knowing the solution conductivity[32-34].

2.4. Characterization of the cell stimulation system

A stimulation system was designed to reproduce the in situ stimuli conditions delivered by capacitive coupling stimulation used in clinics [9, 35]. This system includes three main components: a culture dish electrode assembly (stimulation box, Figs. 1a and 1b); a function generator; and a PC control interface (Fig. 1a). The stimulation box has dishes connected in parallel to accommodate a large number of samples. Every branch of the parallel circuit consists of a set of resistors connected in series,

R1 to R6 (Fig. 1a): R1- known resistor; R2 = R6 - platinum coil immersed in a 20 ml electrolyte solution of KCl (0.33M) housed in a 25 ml plastic container (Polyethylene terephthalate - PET, Kartell); R3 = R5 - salt-bridge filled with Agar (cell culture tested - A1296, Sigma Aldrich)/KCl (0.33M) acting as an electrode (Fig. 1b); R4 - culture medium (α-MEM). Advantageously, the conductive electrodes of biological Agar depress the toxicological/contamination risks to cells by avoiding the release of oxidative species typically formed in metallic electrodes and avoid contamination of other non-metallic electrodes. The extremities of the electrodes (R3 and R5) have a "T" configuration with 5 openings disposed along its length size, with 1 mm in diameter and spaced by 1 cm, to ensure a uniform distribution of the electrical fields and thus a homogeneous stimulation of the samples. Also, the "T" sections of 6 cm in length are smaller than the inner diameter of the culture dish to fit its edge and guarantee the perfect parallelism between electrodes (I and II, Fig. 1c), resembling capacitive coupled electrodes. The maximum number of 6 samples per culture dish was set after obtaining the voltage and current density maps (Figs. 1d and 1e) of the area between the two electrodes (grayish area, Fig. 1c). The maps were obtained in the same conditions of the stimulation experiments using a reference electrode (A) (Fig. 1c) and the equipment described in the previous experimental sections. The area corresponding to the values with the highest uniformity was then selected and used as the stimulation area (delineated with a dotted white line, Figs 1c-e).

2.5. MG63 osteoblastic-like Cell culture

Cell culture: Human osteoblastic-like cells (MG63 cells, ATCC number CRL-1427™) were cultured in α-MEM, supplemented with 10% fetal bovine serum, 50 $\mu g.ml^{-1}$ ascorbic acid, 50 $\mu g.ml^{-1}$ gentamicin and 2.5 $\mu g.ml^{-1}$ fungizone, at 37 ºC, in a

humidified atmosphere of 5% CO_2 in air. For sub-culturing, the cell layer (at around 70-80% confluence) was detached with trypsin – EDTA solution (0.05% trypsin, 0.25% EDTA; 5 minutes, 37ºC). The cell suspension was used in the experiments.

For the cell culture experiments, material samples were provided as square slices of 5×5×1 mm^3, ground and polished (P4000). Before the in vitro testing, the materials were ultrasonically cleaned in ethanol and sterilized by autoclaving.

Cell culture stimulation: The waveform and amplitude of the applied electrical stimuli were carefully selected (Table 1) based on three major requisites for bone electrical stimulation: the time-current-voltage response of Ca^{2+} ion channels of osteoblastic-like cells to an action potential [36]; the current threshold applied in clinic to efficiently stimulate bone tissue - 5-20 μA [9]; and the upper limit of current density and electrical field to avoid tissue injury from heat generation - 1-2 $mA.cm^{-2}$ and 10 $V.cm^{-1}$ [35].

Cells were seeded over standard cell culture coverslips, HA/Glass matrix and CNT/HA/Glass composite at a density of $2x10^4$ $cells.cm^{-2}$. Seeded samples, were cultured for 3 days. At this stage, the culture medium was renewed and the colonized samples were cultured for a further 5 days. During this period, the culture medium was changed twice, and the cultures were exposed to a daily electrical stimulation to one of the following conditions: (i) 5 μA, 15 min, (ii) 5 μA, 30 min, (iii) 15 μA, 15 min, and (iv) 15 μA, 30 min. Symmetrical biphasic square pulses with fixed frequency and duty cycle values of 40 Hz and 20-80% were used, setting action potentials (AP) and resting potential (RP) with fixed periods of 5 and 20 ms (Fig. 1a). This procedure was repeated daily during the 5 days. Cultures were characterized 24 h after 1, 3 and 5 electrical stimuli. Non-stimulated cultures were run in parallel. Cultures were characterized for DNA content, metabolic activity, expression of osteblastic genes and were observed by scanning electron microscopy (SEM) and Confocal Laser Scanning Microscopy (CLSM).

In another experiment, after 3 daily electrical stimuli, the protocol that provided the best stimulation conditions, cultures were maintained for a further 5 days, and were observed by SEM.

DNA content: Non-stimulated and stimulated cultures were evaluated for the DNA content using the PicoGreen DNA quantification assay (Quant-iT™ PicoGreenR dsDNA Assay Kit, Molecular Probes Inc., Eugene. For that, at each time-point, culture medium was removed and the cultures were treated with Triton X-100 (0.1%) (Sigma) to lyse the cell layer. DNA was assessed in the cellular lysates, according to manufacturer´s instructions. Fluorescence was measured on an Elisa reader (Synergy HT, Biotek) at wavelengths of 480 and 520 nm, excitation and emission respectively, and corrected for fluorescence of reagent blanks. The amount of DNA was calculated by extrapolating a standard curve obtained by running the assay with the given DNA standard. Results are expressed as percentage from control.

MTT assay: Metabolic activity of the cell cultures was evaluated by the MTT assay. This is based in the reduction of the MTT (3-(4,5-Dimethylthiazol-2-yl)-2,5-diphenyltetrazolium) by viable cells to a dark blue formazan product. At each time-point, MTT (0.5 $mg.ml^{-1}$) was added to each well, and cultures were incubated for 3 hours at 37ºC. Subsequently, the samples were transferred to new wells, and the formazan salts were dissolved in dimethylsulphoxide (DMSO). In addition, a parallel experiment was run with culture medium, using the same protocol as the cell cultures, to compensate for the background MTT reduction. The optical density (OD) was determined at λ = 600 nm on an Elisa reader (Synergy HT, Biotek). Results are expressed as percentage from control.

Gene expression: Cultures were assessed by RT-PCR after 5 daily stimuli, for the expression of the housekeeping gene glycerol-3-phosphate dehydrogenase (GAPDH), the transcription factor Runx2 and the osteoblastic genes collagen type I

(Col I), alkaline phosphatase (ALP), osteocalcin (OC) and osteoprotegerin (OPG). For that, RNA was extracted with Rneasy® Mini Kit (QIAGEN) according to manufacturer's instructions and was quantified by UV spectrophotometry at 260 nm. Half microgram of RNA was reverse transcribed and amplified (25 cycles) with the Titan One Tube RT-PCR System (Roche), with an annealing temperature of 55ºC. Table 2 shows the primers used in the RT-PCR analysis. After electrophoresis on a 1% (w/V) agarose gel, the bands were analysed by densitometry with ImageJ 1.41 software. Values were normalized to the corresponding GAPDH value of each experimental condition.

SEM and CLSM observation: For SEM observation, samples were fixed (1.5% glutaraldehyde in 0.14 M sodium cacodylate buffer, pH=7.3, 10 min), dehydrated in graded alcohols, critical-point dried, sputter-coated with an Au/Pd thin film (SPI Module Sputter Coater equipment), and observed under a high resolution (Schottky) environmental scanning electron microscope (Quanta 400 FEG ESEM). For confocal laser scanning microscopy (CLSM) assessment, samples were fixed (3.7% paraformaldehyde, 15 min). Cell cytoskeleton filamentous actin (F-actin) was visualized by treating the cells with Alexa Fluor 488 Phalloidin (1:20 dilution in PBS, 1 h) and counterstaining with propidium iodide (1 $\mu g.ml^{-1}$, 10 min) for cell nuclei labelling. Labelled cultures were mounted in Vectashield® and examined under a Leica SP2 AOBS (Leica Microsystems) microscopy.

Statistical analysis: Three independent experiments were performed; in each experiment, three replicas were accomplished for the biochemical assays and two replicas for the qualitative assays. Results are presented as mean ± standard deviation (SD). Groups of data were evaluated using a two-way analysis of variance (ANOVA) and no significant differences in the pattern of the cell behavior were found.

Statistical differences between experimental groups were assessed by Bonferroni's method. Values of $p \leq 0.05$ were considered statistically significant.

3. Results and Discussion

3.1. Microstructural and mechanical characterization of the bone grafts

Bone grafts are expected to restore skeletal integrity by offering biological functional and mechanical supports during bone repairing. To ensure these functionalities, bone grafts scaffolds should fulfill the following main requisites [2]: (1) biodegradable, with non-cytotoxic degradation by-products; (2) mechanical properties close to those of bone and to keep its structural integrity and thus to preserve the porous network during the first stages of the new bone formation. To match this biological profile, it becomes mandatory to control the CNT agglomeration state in the consolidated bioceramic composites. In this respect, a thoroughly characterization of the microstructure and mechanical properties of the materials are reported in the present section.

For the preparation of the composite materials, the hot-pressing temperature of 1100 °C made the glass react with the hydroxyapatite causing its partly conversion into β-TCP (tricalcium phosphate) phase, as depicted in the X-ray diffraction patterns in Figs. 2a and 2b, respectively for the HA/Glass matrix and the 4.4 vol.% CNT/HA/Glass composite. The peaks correspond to those reported in Joint Committee on Powder Diffraction Standards (JCPDS) files for HA (JCPDS 72-1243) and β-tricalcium phosphate, β-TCP (JCPDS 09-0169). Comparing those two plots, it becomes quite clear that there are almost no changes in phase composition when the CNTs are added to the matrix. Arquimedes' density showed that the HA/Glass

matrix is almost fully dense. The scanning electron micrographs (SEM) micrographs of polished surfaces of the unreinforced matrix and the 4.4 vol.% CNT composite after immersion in α-MEM, Figs 2c an 2d, show some well distributed porosity as a result of preferential leaching of the β-TCP phase [37]. This effect is further enhanced in the presence of CNTs, as is clear from the observation of the microstructure of the 4.4 vol.% CNT composite, Fig. 2d. The material surrounding the pore-like defects due to α-MEM preferential attack is less dense, with evidences of micro porosity that is not present in the HA/Glass matrix. Also, from SEM observations only, there are no clearly identifiable zones containing individualized CNTs thereof.

The use of Raman spectroscopy in imaging mode permitted clearly identifying the areas in the dense materials where HA, β-TCP and CNTs are present, as Figs. 2e and 2f illustrate [38]. The image of the unreinforced matrix, Fig. 2e, and the spectra in Fig. 2g help understanding that the pore-like defects are associated to the β-TCP phase location. Also, there is carbon contamination during hot-pressing in graphite dies at temperatures where the HA/Glass matrix is quite chemically active. This contamination is not so clear in the Raman mapping of Fig. 2f, for the 4.4 vol.% CNT composite. Combining the code colors in Fig. 2f with the corresponding spectra in Fig. 2h, it becomes clear that CNTs (addressed by the G' (2D) signature and higher G/D ratio) are present mainly as elongated agglomerates but can be identified throughout the matrix, within the resolution limits of the technique. It is worth noting that the observed SEM surfaces are parallel to the pressing direction, this accounting for the pressure induced alignment observed of the CNT large agglomerates in the 4.4 vol.% CNT material (Fig. 2d). The 6% porosity measured in this material by Arquimedes' immersion reflects not only the damping effect of the CNTs and the difficulty in transmitting the pressure to the HA/Glass matrix for densification, but also the increased interactions and entanglement of CNT agglomerates that further prevent

matrix contiguity from happening. This porosity is closer to the cortical bone than the Glass/HA matrix alone, that is almost fully dense but still reacts readily with α-MEM, as shown above, Fig. 2c. Nevertheless, both the compressive and bending strength of the produced materials have values that are well within or above cortical bone specifications for adult, healthy individuals with average values of compressive and bending strengths of 700 MPa and 160 MPa, respectively, for the 4.4 vol.% CNT/HA/Glass composite.

3.2. Bone grafts-α-MEM culture medium interactions

A key idea of the present work is to make the electrical stimulus to converge through the osteoblasts present at the composite surface in order to tune its cellular functions. Fig. 3a gives the conductivity of the culture medium α-MEM and several biological tissues/organs/milieus together with the new CNT/Glass/HA material (labeled at blue)[39]. It can be seen that the CNT composite has higher conductivity than the in vitro culture medium and than any in vivo environment. In line with this, it is expectable that this characteristic yields CNTs containing substrates with high potential to increase the local conductivity and to confine electrical fields, making them high efficient electron transport and delivering pathway systems.

To ensure the validity of this hypothesis and the experimental approach used for cell stimulation, a set of preliminary studies were carried out, as follows: (1) by studying the effects on the overall resistivity of α-MEM using immersed conducting and nonconducting samples; and (2) by identifying the current density (electric field) lines on samples of different geometries.

3.2.1. Neutral conditions

The electrochemical cells contained α-MEM and 6 or 12 samples (example in Fig. 3b). The impedance of the cell was measured in a two electrode arrangement using 2 platinum spiral electrodes. The variation of the modulus of impedance, |Z|, with the signal frequency is shown in Fig. 3c. The values are normalized to the area of the electrodes. The impedance response shows two regions, one at higher frequencies with constant |Z| and another at frequencies below ~5 kHz where |Z| increases as the frequency decreases. The high frequency region is related to the solution resistance while the second one measures the double layer capacitance at the surface of the Pt electrodes. As so, only the high frequency part is interest to this study.

The control curve is simply the resistance of α-MEM. The other curves give the resistance when 6 or 12 samples of either Glass/HA (non-conductive) or CNT/Glass/HA (conductive) were immersed in solution. It increased with 12 nonconductive samples and decreased when conductive pieces were used, with a decrease proportional to the number of pieces. The same experiment with different materials showed that the more conductive the material is the lower the resistance of the medium.

3.2.2. Electrical stimulation conditions

The current lines in solution near the conductive samples, when placed in an electrochemical cell, were measured by a vibrating voltage probe. Fig. 4a depicts the experimental set up with a fixed current running from one electrode plate to the other, both disposed in parallel. Part of the current flows through the sample and the remaining current will diverge, surrounding the sample, because it represents an obstacle to flow. A component of the current normal to the surface could be detected,

having a positive sign on the side of the positive electrode because the current lines shift up and negative on the right because the current paths descend, returning to their original path in the solution, as can be seen in Fig. 4b. The closer the line of measurement is to the sample the higher is the measured normal component. A distance of 50 μm provided the highest sensitivity to the normal current, still avoiding the risk of the probe touching the sample. The experiment was repeated with different materials, Fig. 4c. The decrease of the normal component for higher conductive materials proves that the current is converging through the material in a higher extent for the more conductive materials (steel and graphite).

The influence of the sample geometry on current distribution was also investigated because CNT/Glass/HA bone grafts may be applied as granules having irregular shapes, thus being important to check if geometry is a factor to consider in the electrical field distribution. The results in Fig. 5 show that no significant differences of the z component of current density, $I_{z,}$ exist for triangular, round and rectangular shaped samples. Also, the correspondent I_z values for CNT/Glass/HA and Glass/HA samples are close, still, the former have lower values, corroborating data of Fig. 5b.

3.3. Osteoblastic cells proliferation and gene expression: substrate efficiency in in situ stimulus delivery

MG63 cell line was used to address the potential role of the electroconductivity of the CNT/HA/Glass composite on the osteoblastic cell response under electrical stimulation, and to select an optimized set of conditions for improved cell behaviour. This cell system provides a homogeneous, phenotypically stable and proliferative population that shows many phenotypic features of normal osteoblastic cells including hormonal responsiveness and expression of early and late stage

osteogenic genes, being widely used as a osteoblast cell model for *in vitro* research [40]. Cell cultures, performed on standard cell culture coverslips, HA/Glass matrix and CNT/HA/Glass composite were submitted to electrical stimuli of 5 μA/15 min, 5 μA/30 min, 15 μA/15 min or 15 μA/30 min (Table 1), one time a day for up to five consecutive days, and were assessed 24 h after 1, 3 and 5 stimuli for the DNA content, metabolic activity and gene expression of Runx2 (Runt-related transcription factor 2), Col I (Collagen type I), ALP (Alkaline Phosphatase), OC (Osteocalcin) and OPG (Osteoprotegerin).

The DNA content on the cultured coverslip and on the two materials, in non-stimulated conditions, increased throughout the culture time. This parameter reflects the number of cells present on the substrates, being an index of the cell proliferation. Under electrical stimulation, DNA content on the CNT/HA/Glass composite was greatly increased after 1 and 3 stimuli (~25 to 60%) and was similar after 5 days of treatments, compared to non-stimulated cultures (Fig. 6c). The inductive effect was dependent on the stimulus intensity and duration, and was higher with 15 μA, 30 min (after 1stimulus, ~60%) and 15 μA, 15 min (after 3stimuli, ~62%). Cell response over the dielectric surfaces (coverslip and HA/Glass matrix) was similar under electrical stimulation (Figs. 6a and 6b). Compared to non-stimulated cultures, DNA content was slightly increased, similar and significantly lower after 1, 3 and 5 daily treatments. Results for the MTT reduction (Figs. 6d-f), a metabolic activity/proliferation assay based on the reduction ability of cell mitochondrial dehydrogenases, showed a pattern similar to that observed for the DNA content, in the conductive and dielectric substrates. However, in both types of surfaces, for the inductive effects, the percentage of increase of the OD values reflecting the metabolic activity was always higher than that found for the DNA content. Thus, on the CNT/HA/Glass composite,

increases of ~40 to 130% were found after 1 and 3 stimuli. Hence, under selected stimulation conditions, both the cell proliferation and the metabolic activity were induced, suggesting the presence of a higher number of cells with increased metabolic activity, compared to non-stimulated conditions. However, these cellular parameters decreased following repeated stimuli. This behaviour has been previously reported and appears to be conditioned by the stage of cell differentiation [41, 42].

Cultures were characterized for the mRNA expression of several osteoblastic genes, 24h after 5 daily electrical stimuli, under 15 μA, 15 min (Fig. 7). Results show that the expression of Runx2 was particularly sensitive to the inductive effects of the electrical stimulation. It was up-regulated on the cultures grown over the CNT/HA/Glass composite, and also on those over the HA/Glass matrix. Even in the cultured coverslip, that showed low expression of Runx2 in the non-stimulated cultures, there was a trend for an increase under stimulation conditions. This is an interesting finding, as Runx2 is the earliest transcription factor for osteogenic differentiation and, in addition, it activates the expression of multiple late stage osteoblastic genes[35]. Over the stimulated CNT/HA/Glass composite, there was also increased mRNA expression for ALP and OC, respectively an early and a late stage marker in the osteogenic differentiation pathway. As both molecules have a role in the extracellular matrix mineralization, respectively in the initiation of mineral deposition (ALP) and in the regulation of crystal growth (OC)[43], this observation points to an enhanced osteogenic differentiation under electrical stimulation. No effect was noted on the expression of Col 1 and OPG. Col 1 is the most abundant extracellular bone matrix, being considered an early bone differentiation marker, which has a role in osteoblastic differentiation and also in the nucleation site and growth space of hydroxyapatite [44, 45]. On the other hand, OPG is a key molecule in the interplay between osteoblasts and osteoclasts during bone remodelling. It is a decoy receptor

that binds to RANKL, blocking its binding to the RANK receptor on osteoclasts, inhibiting osteoclastogenesis[46]. These results on the gene expression might suggest that electrical stimulation induces the osteogenic differentiation and, eventually, may also enhance the level of matrix mineralization of the collagenous extracellular matrix. Additionally, the osteoblast/osteoclast interactions regarding the modulation of osteoclastogenesis *via* OPG appear not to be affected. Overall, such a profile would be interesting to speed up the initial material stabilization leading to a faster osseointegration process.

On CLSM (Fig. 8), non-stimulated and stimulated cells (observed 24h after 1 and 3 daily electrical stimuli, 15 μA/15 min) displayed a polygonal/elongated morphology on the HA/Glass matrix and, essentially, an elongated/fusiform appearance on the CNT/HA/Glass composite. In both surfaces, cells exhibited a well-organized F-actin cytoskeleton, with intense staining at the cell boundaries, prominent nucleus and on-going cell division, signs of mechanical integrity and healthy behaviour. Over the CNT/HA/Glass composite, a specific cell orientation was visible already at day 1, and a characteristic aligned cell growth was evident at later culture times, compared to the random pattern of cell growth seen over the HA/Glass matrix. SEM observation of the same cultures (Fig. 9a) provided similar information but, additionally, images showed that the organization of the cell layer over the CNT/HA/Glass composite followed the alignment direction of the CNT agglomerates on the Glass/HA matrix. This behaviour was evident since the beginning of the culture time, as seen 24h after 1 electrical stimulus, and also over longer culture times, i.e. 24h after 3 electrical stimuli. Cultures were also observed 5 days after 3 daily electrical stimuli, 15 μA/15 min. SEM images showed an abundant and well-organized cell layer over the three surfaces, evidencing that cell proliferation increased with the culture time. Also, cells presented a healthy morphology and intimate cell-to-cell contact. Representative

images of the stimulated cultures are shown in Fig. 9b, and it is worthy to note that the cultures grown over the CNT/Glass/HA composites still maintained a well-defined alignment. Additionally, a high magnification SEM image showed a close interaction between the surface of a well spread cell and the CNT network on the composite structure.

This observation is in line with some reported information, showing that aligned CNT networks exhibited the ability to modulate cell morphology and the directional growth of human osteoblastic cells, in comparison to seeded randomly oriented CNT network [47, 48]. Overall, the electrical stimulation did not result in evident effects in the aligned cell organization over the CNT/HA/Glass composite. The distinct cytoskeleton organization over the CNT/HA/Glass and HA/Glass samples is expected to modulate the cell response to the two substrates. The F-actin cytoskeleton, which is highly concentrated just beneath the plasma membrane, provides structural stability and elasticity to the cell undergoing substrate adaptation, but it is also a key player in the cellular mechano-transduction mechanisms modulating complex signalling pathways, such as Rho family GTPases, which affects the overall cell behaviour [49]. Related to this, it has been suggested that the directional cell growth observed in aligned CNTs structures enhances osteogenic differentiation, in comparison to seeded randomly oriented CNTs network, a process possibly mediated by the high cytoskeleton tension accumulated on aligned cells leading to the activation of selective mechano-transduction pathways [48].

Results showed that under an appropriate electrical stimulation protocol, the conductive CNT/HA/Glass composite exhibited significantly improved cell proliferation, metabolic activity and osteoblastic gene expression. The lower inductive effect on cell proliferation but higher expression of relevant osteogenic genes and ALP activity found over the CNT/HA/Glass composite after few stimuli suggest an

inductive effect on the osteoblastic differentiation, taking into account the established reciprocal relationship between proliferation and differentiation during the development of the osteoblastic phenotype [44].

Briefly, cell functional activity was significantly improved on the CNT/HA/Glass composite, which is intimately related with its efficiency in the electrical stimuli delivering to cells. According to section 3.2, conductive substrates increase the local conductivity of the culture medium and render the confinement of the exogenous electrical fields on the surface of the material. Fig. 10 sketches the interaction of the electrical field lines with cells surrounding non-conductive and conductive substrates. In the latter, the electrical field confinement (higher current density) at perpendicular angles to the surface[39] imposes osteoblastic cells in contact to be crossed by the electrical fields. Contrarily, in a dielectric material the external fields are parallel to its surface, so they are not confined, thus a much lower efficiency of stimuli delivering at the sample surface is observed relatively to the conductor material.

Regarding the involved mechanisms, electrical stimulation seems to modulate cell behaviour essentially by altering the intracellular calcium dynamics [49]. Although being a versatile process and likely to depend on the cell type and microenvironmental conditions, the modulation of the intracellular calcium levels in human mesenchymal stem cells seems to be involved in directing their osteogenic differentiation [49-51]. Associated mechanisms appear to be related with the clustering and activation of cell-surface receptors (e.g. integrins), interaction with G-protein coupled receptors (e.g., PLC - Phospholipase C), ATP (Adenosine 5'- triphosphate) release and activation of ion channels. Regarding the latter, the intracellular calcium can be raised inside osteoblastic cells by Ca^{2+} transport via L-type Ca^{2+} channels [52, 53]. Of interest, it was found that these ion channels preferentially regulate Ca^{2+}-dependent genes and enzymes, such as the Ca^{2+}/calmodulin-dependent protein kinase II

(CaMKII)[54], a key pathway towards regulation of osteoblast proliferation/differentiation [55]. In the present work, the high current-voltage thresholds of osteoblastic Ca^{2+} ion channels give further evidences that cell response to stimuli appears to be L-type Ca^{2+}/CaMKII mediated since cell proliferation and metabolic activity were maximized for the high current stimuli conditions (15 μA,15 min). Moreover, compared to Glass/HA, the conductive CNT/Glass/HA composite reveals a higher activation of L-type ion channels (i.e. intracellular Ca^{2+} levels) and further larger efficiency of bone cell stimulation. This may be related to the high efficiency of charge transfer voltage at the substrate-cell interface, related to the high density of electric field lines crossing the cell (Fig. 10), which boosts opening of voltage-gated channels at multi-locations in the cell membrane, and raises action potentials' magnitude.

4. Conclusions

In the present study, the conductive CNT/HA/Glass composite showed significantly improved cell functional activity under an appropriate electrical stimulation protocol, compared to the HA/Glass matrix. The cell metabolic activity and DNA content were increased by 130% and 60%, relatively to the non-stimulated condition, after only 3 days of daily stimulation of 15 μA for 15 min. Moreover,the osteoblastic gene expression for Runx2, OC and ALP was enhanced by 80%, 50% and 25%, after 5 days of stimulation. These observations were intimately related to the local increase of the culture medium conductivity and the confinement of electrical fields on the surface of the conductive material. It is trust that experimental evidences of selective bone cell stimulation on conductive bone grafts will offer new possibilities in non invasive clinic electrotherapies.

Acknowledgements

D. Mata acknowledges Foundation for Science and Technology (FCT, Portugal) for funding the project PEst-C/CTM/LA0011/2013.

References

[1]. M. M. Stevens. *Mater Today,* 2008, **11**, 18-25.

[2]. M. Navarro; A. Michiardi; O. Castaño; J. A. Planell. *J R Soc, Interface,* 2008, **5**, 1137-58.

[3]. R. Spear; R. Cameron. *International Journal of Material Forming,* 2008, **1**, 127-33.

[4]. C. A. L. Bassett; R. O. Becker. *Science,* 1962, **137**, 1063-4.

[5]. I. Yasuda. *J Jpn Orthop Surg Soc,* 1954, **28**, 267-71.

[6]. C. Bassett. *Crit Rev Bioeng,* 1989, **17**, 451-529.

[7]. M. Zayzafoon. *J Cell Biochem,* 2006, **97**, 56-70.

[8]. F. Bezanilla. *Physiol Rev,* 2000, **80**, 555-92.

[9]. M. Griffin; A. Bayat. *Eplasty,* 2011, **11**.

[10]. M. Griffin; S. Iqbal; A. Sebastian; J. Colthurst; A. Bayat. *Journal of Bone & Joint Surgery, British Volume,* 2012, **94-B**, 33.

[11]. D. G. Woo; M.-S. Shim; J. S. Park; H. N. Yang; D.-R. Lee; K.-H. Park. *Biomaterials,* 2009, **30**, 5631-8.

[12]. Z. Schwartz; B. J. Simon; M. A. Duran; G. Barabino; R. Chaudhri; B. D. Boyan. *Journal of Orthopaedic Research,* 2008, **26**, 1250-5.

[13]. M. Akai; K. Hayashi. *Bioelectromagnetics,* 2002, **23**, 132-43.

[14]. W. M. Novicoff; A. Manaswi; M. V. Hogan; S. M. Brubaker; W. M. Mihalko; K. J. Saleh, *Critical Analysis of the Evidence for Current Technologies in Bone-Healing and Repair*. 2008; Vol. 90, p 85-91.

[15]. S. B. Behrens; M. E. Deren; K. O. Monchik. *Current Orthopaedic Practice,* 2013, **24**, 84-91

[16]. P. R. Supronowicz; P. M. Ajayan; K. R. Ullmann; B. P. Arulanandam; D. W. Metzger; R. Bizios. *Journal of Biomedical Materials Research,* 2002, **59**, 499-506.

[17]. S. Meng; M. Rouabhia; Z. Zhang. *Bioelectromagnetics,* 2013, **34**, 189-99.

[18]. S. Orrenius; B. Zhivotovsky; P. Nicotera. *Nat Rev Mol Cell Biol,* 2003, **4**, 552-65.

[19]. G. Ermak; K. J. A. Davies. *Mol Immunol,* 2002, **38**, 713-21.

[20]. D. A. Puleo; W. W. Huh. *J Appl Biomater,* 1995, **6**, 109-16.

[21]. J. Zhang; K. G. Neoh; X. Hu; E.-T. Kang; W. Wang. *Biotechnol Bioeng,* 2013, **110**, 1466-75.

[22]. K. Sahithi; M. Swetha; K. Ramasamy; N. Srinivasan; N. Selvamurugan. *International Journal of Biological Macromolecules,* 2010, **46**, 281-3.

[23]. M. Vila; M. Cicuéndez; J. Sánchez-Marcos; V. Fal-Miyar; M. Manzano; C. Prieto; M. Vallet-Regi. *J Biomed Mater Res, Part A,* 2013, **101A**, 213-21.

[24]. S. Facca; D. Lahiri; F. Fioretti; N. Messadeq; D. Mainard; N. Benkirane-Jessel; A. Agarwal. *ACS Nano,* 2011, **5**, 4790-9.

[25]. D. Lahiri; V. Singh; A. K. Keshri; S. Seal; A. Agarwal. *Carbon,* 2010, **48**, 3103-20.

[26]. C. A. Poland; R. Duffin; I. Kinloch; A. Maynard; W. A. Wallace; A. Seaton; V. Stone; S. Brown; W. MacNee; K. Donaldson. *Nat Nanotechnol,* 2008, **3**, 423-8.

[27]. J. Meng; L. Song; H. Kong; G. Zhu; C. Wang; L. Xu; S. Xie; H. Xu. *J Biomed Mater Res, Part A,* 2006, **79A**, 298-306.

[28]. M. A. Correa-Duarte; N. Wagner; J. Rojas-Chapana; C. Morsczeck; M. Thie; M. Giersig. *Nano Letters,* 2004, **4**, 2233-6.

[29]. D. A. LaVan; T. McGuire; R. Langer. *Nat Biotechnol,* 2003, **21**, 1184-91.

[30]. D. Mata; F. J. Oliveira; N. M. Ferreira; R. F. Araújo; A. J. S. Fernandes; M. A. Lopes; P. S. Gomes; M. H. Fernandes; R. F. Silva. *Nanotechnology,* 2014, **25**, 145602.

[31]. D. Mata; A. L. Horovistiz; I. Branco; M. Ferro; N. M. Ferreira; M. Belmonte; M. A. Lopes; R. F. Silva; F. J. Oliveira. *Materials Science and Engineering: C,* 2014, **34**, 360-8.

[32]. L. F. Jaffe; R. Nuccitelli. *The Journal of cell biology,* 1974, **63**, 614-28.

[33]. C. Scheffey. *Review of Scientific Instruments,* 1988, **59**, 787-92.

[34]. B. Reid; R. Nuccitelli; M. Zhao. *Nature protocols,* 2007, **2**, 661-9.

[35]. B. M. Isaacson; R. D. Bloebaum. *J Biomed Mater Res, Part A,* 2010, **95A**, 1270-9.

[36]. J. Loza; E. Stephan; C. Dolce; R. Dziak; S. Simasko. *Calcified Tissue International,* 1994, **55**, 128-33.

[37]. S. Jalota; S. B. Bhaduri; A. C. Tas. *J Biomed Mater Res, Part A,* 2006, **78A**, 481-90.

[38]. R. Cuscó; F. Guitián; S. d. Aza; L. Artús. *J Eur Ceram Soc,* 1998, **18**, 1301-5.

[39]. S. Grimnes; G. Martinsen, *Bioimpedance and Bioelectricity Basics*. Academic Press: UK, 2008.

[40]. E. Czekanska; M. Stoddart; R. Richards; J. Hayes. *Eur Cell Mater* 2012, **24**, 1-17.

[41]. J. Jansen; O. van der Jagt; B. Punt; J. Verhaar; J. van Leeuwen; H. Weinans; H. Jahr. *BMC Musculoskeletal Disord,* 2010, **11**, 188.

[42]. M.-T. Tsai; W.-J. Li; R. S. Tuan; W. H. Chang. *J Orthop Res,* 2009, **27**, 1169-74.

[43]. P. T. O'Donnell; V. L. Collier; K. Mogami; S. I. Bernstein. *Genes Dev,* 1989, **3**, 1233-46.

[44]. J. E. Aubin, Mesenchymal stem cell and osteoblast differentiation, in Principles of bone biology In *Principles of bone biology*, R. L. Bilezikian JP, Martin TJ, Ed. Academic Press: USA, 2008; Vol. 1.

[45]. H. K. Datta; W. F. Ng; J. A. Walker; S. P. Tuck; S. S. Varanasi. *Journal of Clinical Pathology,* 2008, **61**, 577-87.

[46]. K. Matsuo; N. Irie. *Archives of Biochemistry and Biophysics,* 2008, **473**, 201-9.

[47]. S. Giannona; I. Firkowska; J. Rojas-Chapana; M. Giersig. *J Nanosci Nanotechnol,* 2007, **7**, 4-5.

[48]. S. Namgung; K. Y. Baik; J. Park; S. Hong. *ACS nano,* 2011, **5**, 7383-90.

[49]. I. Titushkin; S. Sun; J. Shin; M. Cho. *Biomed Res Int,* 2010, **2010**.

[50]. S. Sun; Y. Liu; S. Lipsky; M. Cho. *The FASEB Journal,* 2007, **21**, 1472-80.

[51]. I. Titushkin; M. Cho. *Biophys J,* 2007, **93**, 3693-702.

[52]. S. E. Guggino; J. A. Wagner; A. M. Snowman; L. D. Hester; B. Sacktor; S. H. Snyder. *J Biol Chem,* 1988, **263**, 10155-61.

[53]. D. Chesnoy-Marchais; J. Fritsch. *J Physiol,* 1988, **398**, 291-311.

[54]. B. Z. Peterson; C. D. DeMaria; D. T. Yue. *Neuron,* 1999, **22**, 549-58.

[55]. M. Zayzafoon. *J Cell Biochem,* 2006, **97**, 56-70.

List of Captions

Table 1. *In vitro* electrical stimulation metrics of human osteoblastic cells.

Table 2. Primers used on RT-PCR analysis.

Fig. 1 (a) Schematic illustration of the electrical stimulation system: stimulation box; function generator, with the respective waveform used (action potentials - AP and resting potentials - RP); and PC control interface. (b) Photograph image of the stimulation box. (c) Magnified photograph image of a culture dish of (b) with parallel disposed salt-bridge electrodes. Color maps of the (d) voltage and (e) current density of the stimulation zone (delineated by a white dotted line).

Fig. 2 XRD spectra of hot-pressed (a) Glass/HA and (b) CNT/Glass/HA compacts. (■ β-TCP, ▲ HA) (c and d) SEM micrographs of (a) and (b). (e and f) Colour Raman maps and respective (g and h) spectra of (a) and (b) (carbon and CNTs: ● D-band, ★ G-band, ⬣ G'(2D)-band; *β*-TCP: ◆v_1-PO_3^{2-} , ⬟v_2-PO_3^{2-}; HA: ◆v_1-PO_3^{2-} , ▼v_2-PO_3^{2-}).

Fig. 3 (a) Plot comparing the electrical conductivity of biological tissues and milieus[39], α-MEM and the CNT/Glass/HA composite (highlighted at blue). (b) Photographs of the electrochemical cells with 6 samples immersed in 12 ml of α-MEM and platinum spiral electrodes. (c) Plots showing the dependence of the modulus of impedance |Z| of the electrochemical cells on the signal frequency.

Fig. 4 (a) Set-up of the vibrating voltage probe measuring system of a electrochemical cell containing one sample immersed in 12 ml of α-MEM and parallel

graphite electrodes (b) Plot of the variation of the current density line profile (from I to II labels) in the z direction with the distance between the surface of the sample and the vibrating probe of (a). (c) Plot showing the influence of the electrical conductivity of the sample on the current density line profiles at a fixed sample-probe distance of 50 μm.

Fig. 5 (a) Photographs showing the 2D distribution of the current density vectors (I_x, I_z) for CNT/Glass/HA samples with different edge geometries. Respective plots of the variation of the current density line profiles in the (b) z direction with the edge geometry of Glass/HA and CNT/Glass/HA samples.

Fig. 6 (a-c) DNA content and (d-f) cell viability/proliferation of osteoblastic cell cultures grown over standard cell culture coverslips, Glass/HA matrix and CNT/Glass/HA composite, and characterized 24h after 1, 3, and 5 daily electrical stimuli, under different stimulation conditions. Results are expressed as percentage of variation from non-stimulated cultures. *Significantly different from non-stimulated cultures.

Fig. 7 Expression of osteoblastic-related genes by cell cultures grown over standard cell culture coverslips, Glass/HA matrix and CNT/Glass/HA composite, and characterized 24h after 5 daily electrical stimuli, under 15 μA, 15 min. Results are expressed as percentage of variation from non-stimulated cultures. Densitometric analysis of the RT-PCR bands normalized to the corresponding GAPDH value (a, c, e) and representative images of the PCR products in the agarose gel (b, d, f). *Significantly different from non-stimulated cultures.

Fig. 8 CLSM appearance of osteoblastic cell cultures grown over Glass/HA matrix and CNT/Glass/HA composite, and observed 24h after 1 and 3 daily electrical stimuli, under different stimulation conditions. Cells were stained for F-actin cytoskeleton (green) and nucleus (red).

Fig. 9 (a) SEM appearance of osteoblastic cell cultures grown over standard cell culture cover slips, Glass/HA composite and CNT/Glass/HA composite, and observed 24h after 1 and 3 daily electrical stimuli, 15 μA/15 min. (b): SEM appearance of the cultures observed 5 days after the 3 daily electrical stimuli, 15 μA/15 min; the panel also displays a high magnification image of the CNT/Glass/HA composite showing a close interaction between the osteoblastic cells and the CNT on the composite matrix.

Fig. 10 Top view schematic images of the electric field (current density) lines distribution of a (a) dielectric and a (b) conductive spherical samples interfacing with osteoblastic cells (elliptical purple sketches) immersed in a homogeneous α-MEM culture medium.

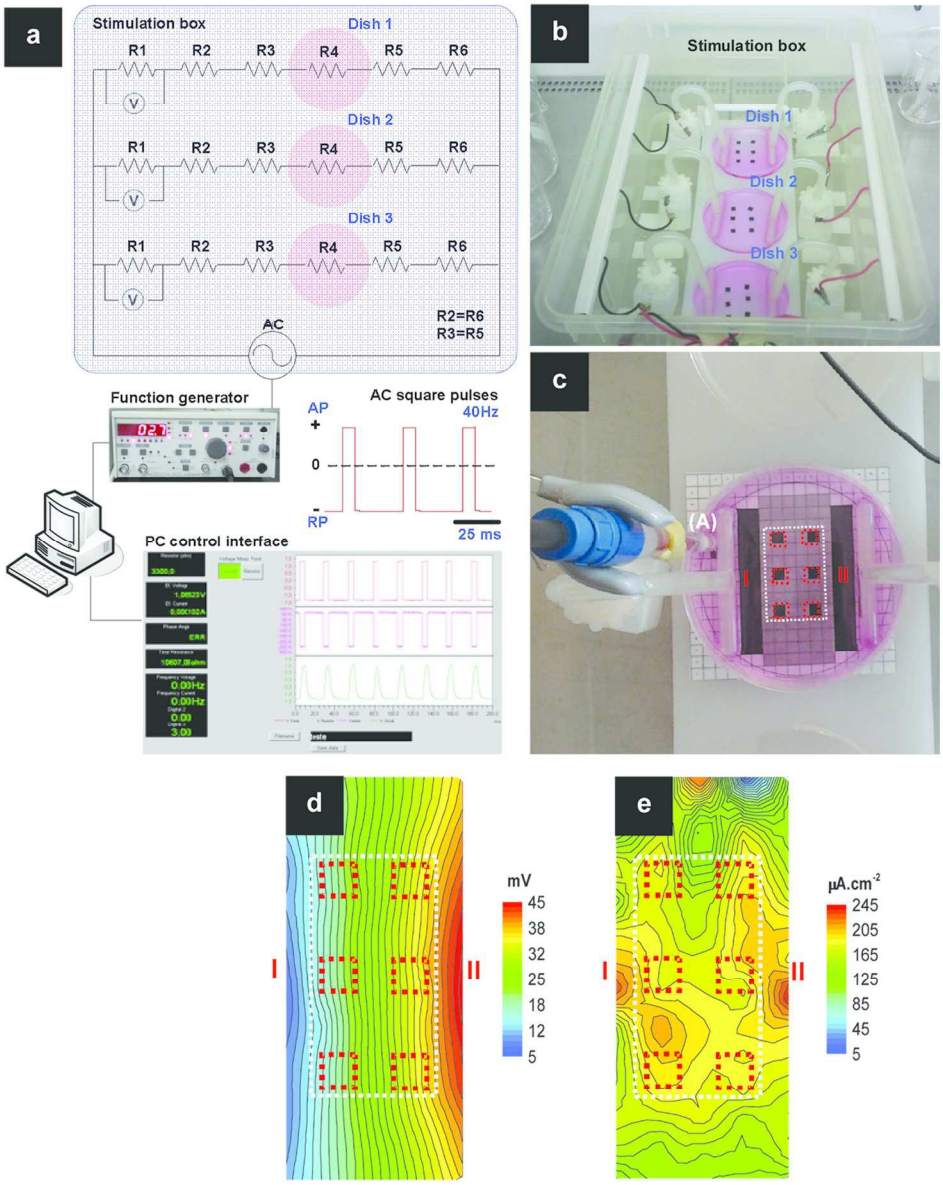

140x175mm (300 x 300 DPI)

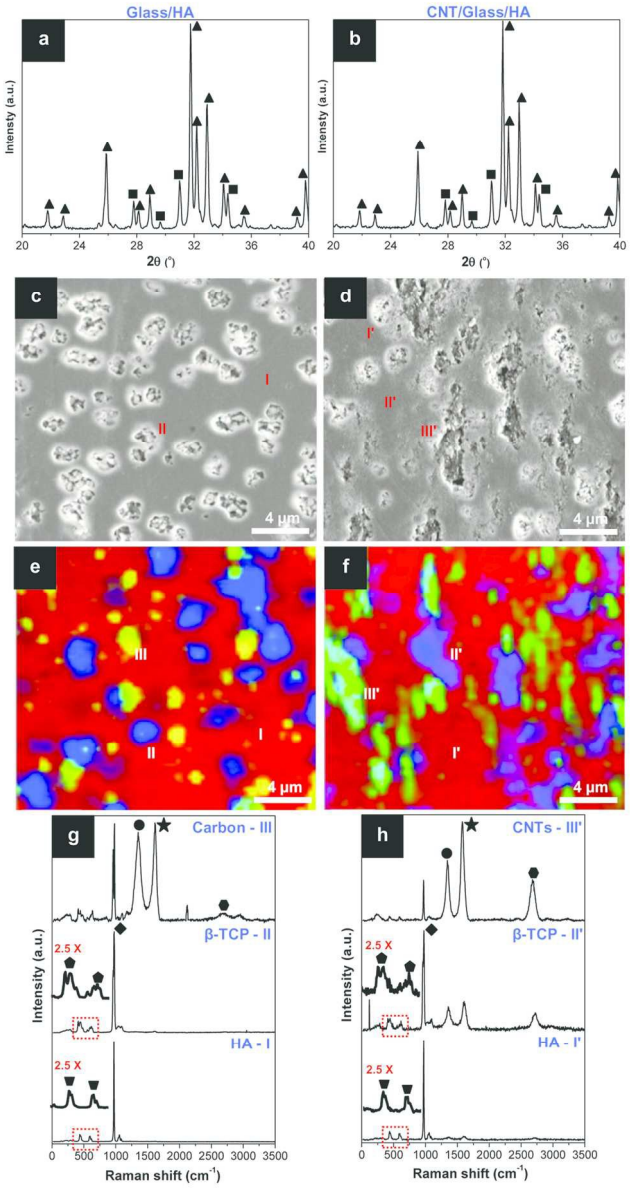

109x202mm (300 x 300 DPI)

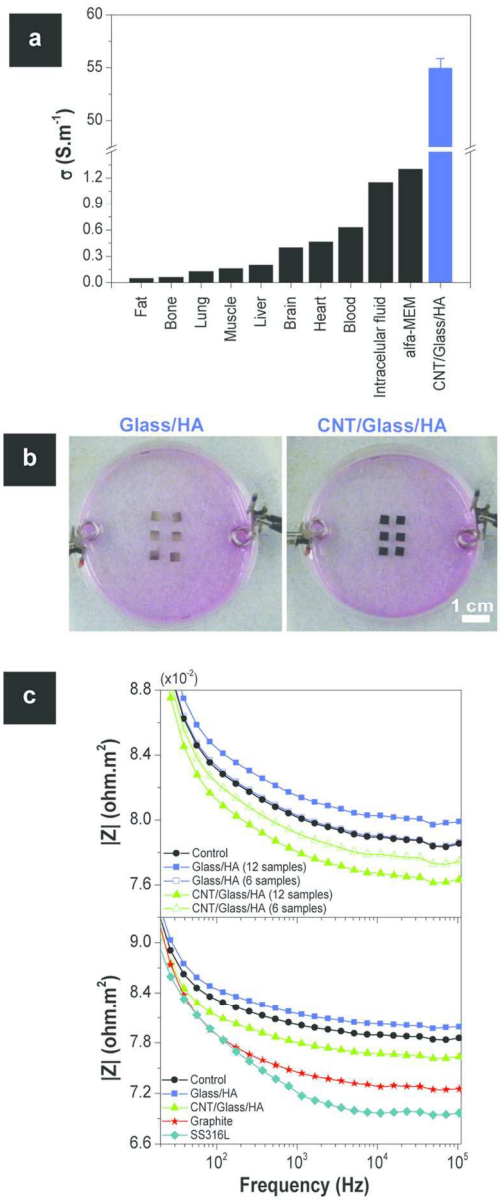

80x186mm (300 x 300 DPI)

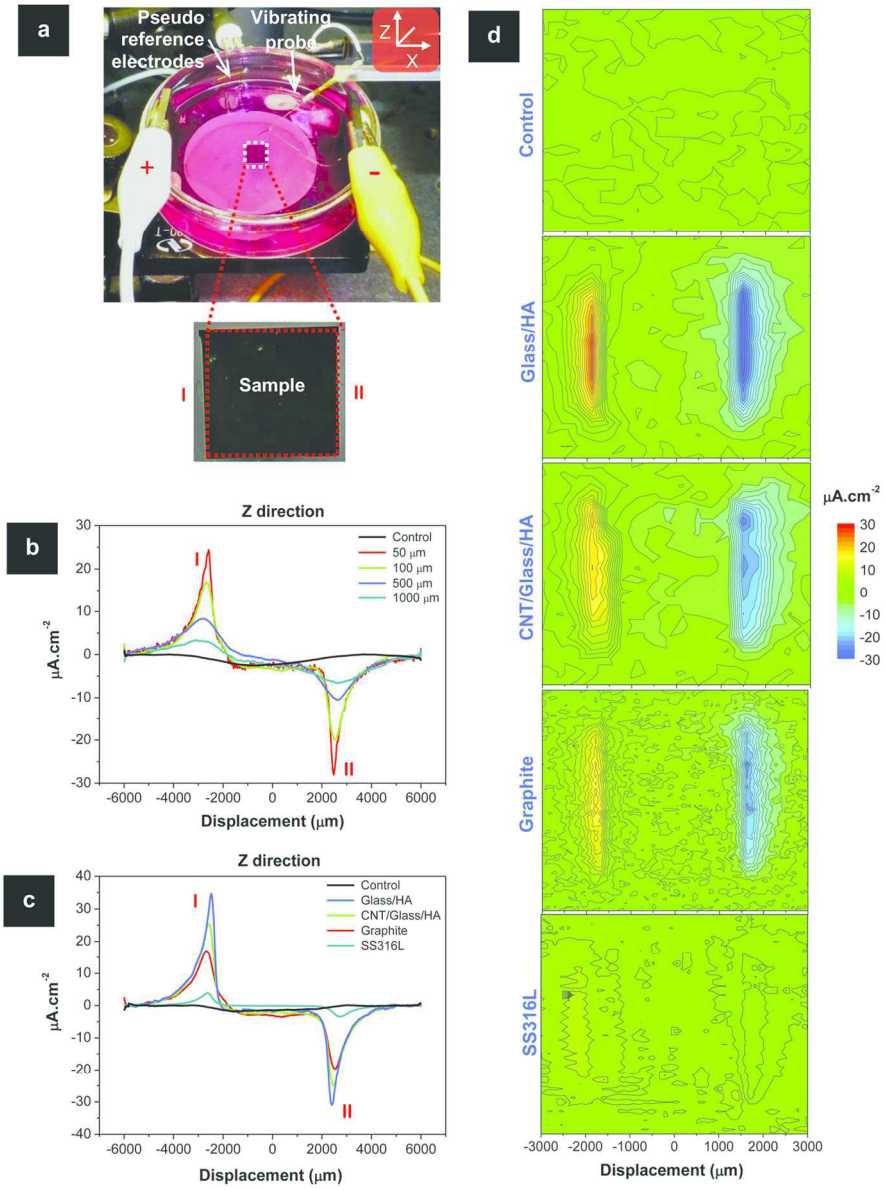

129x175mm (300 x 300 DPI)

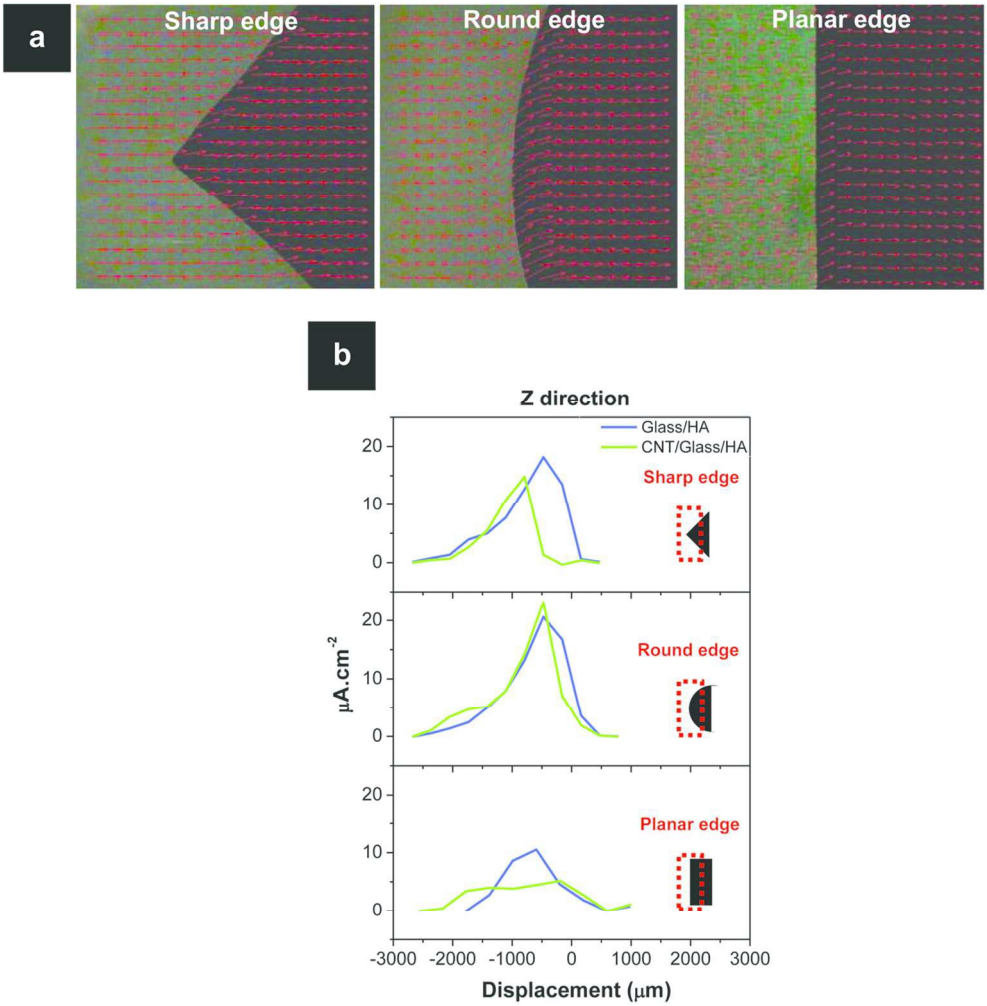

119x122mm (300 x 300 DPI)

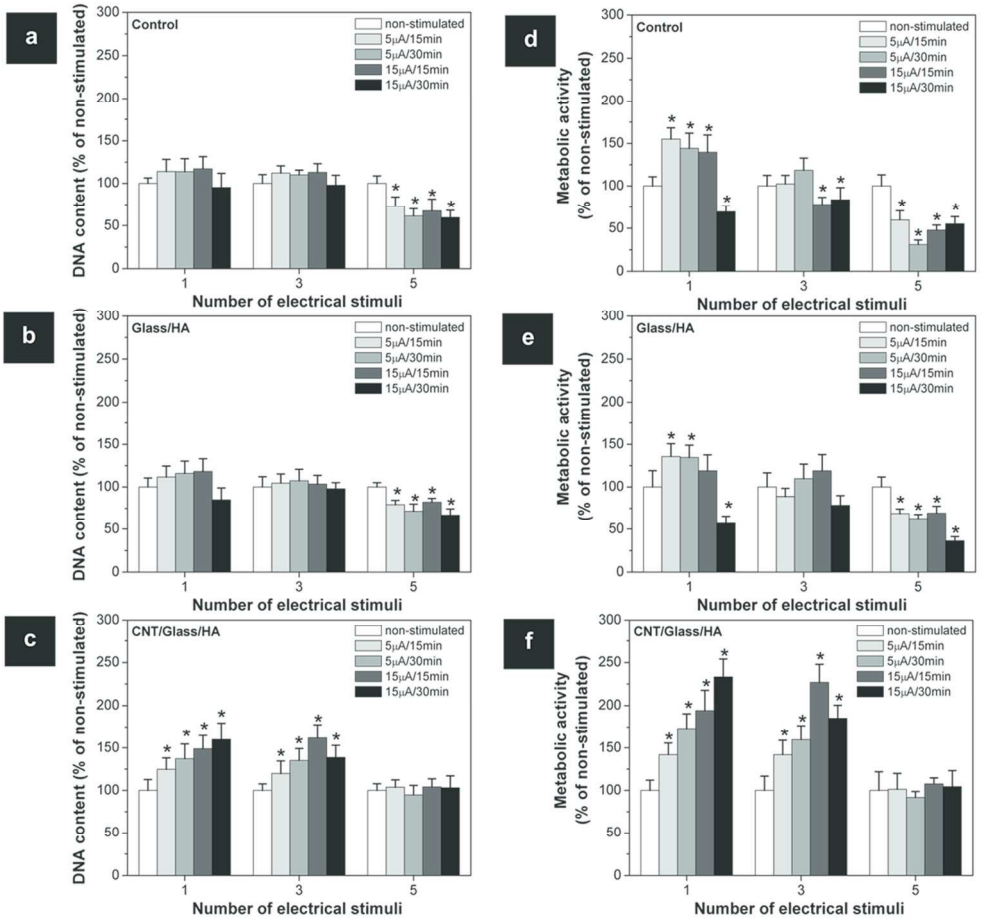

109x103mm (300 x 300 DPI)

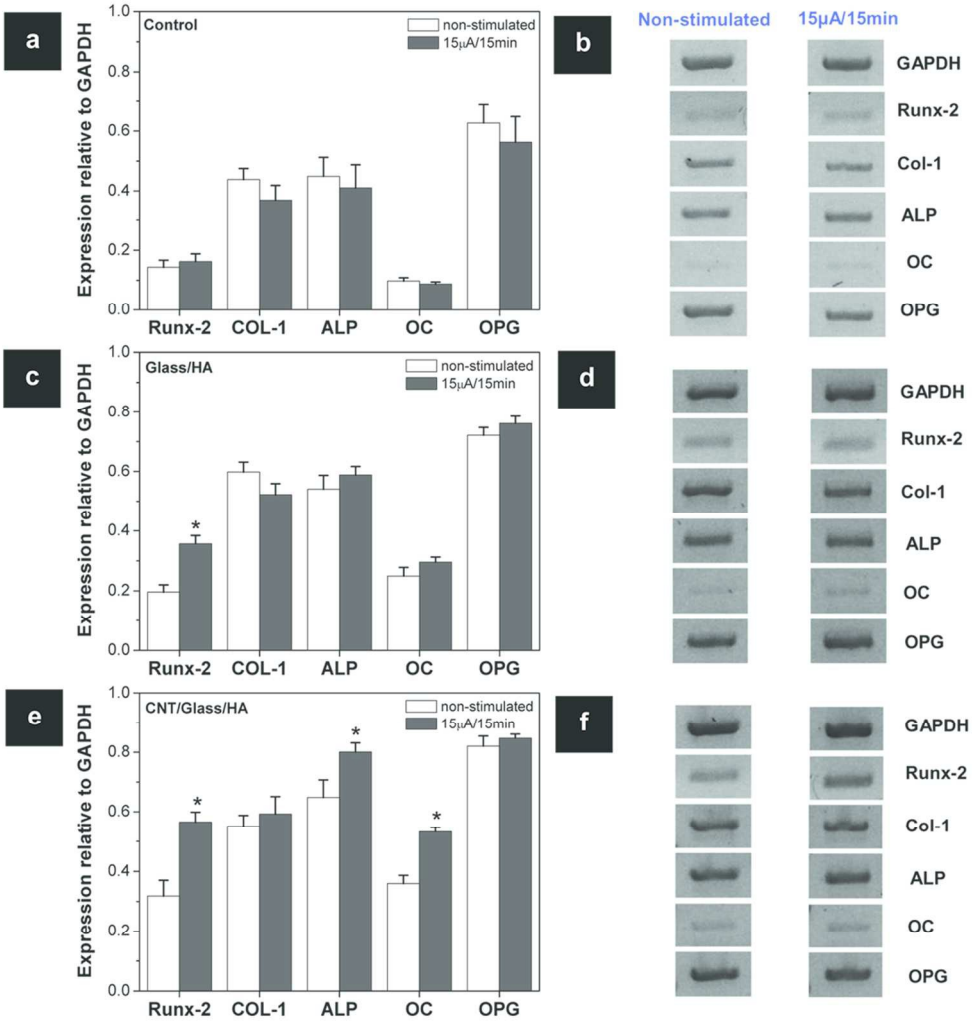

109x115mm (300 x 300 DPI)

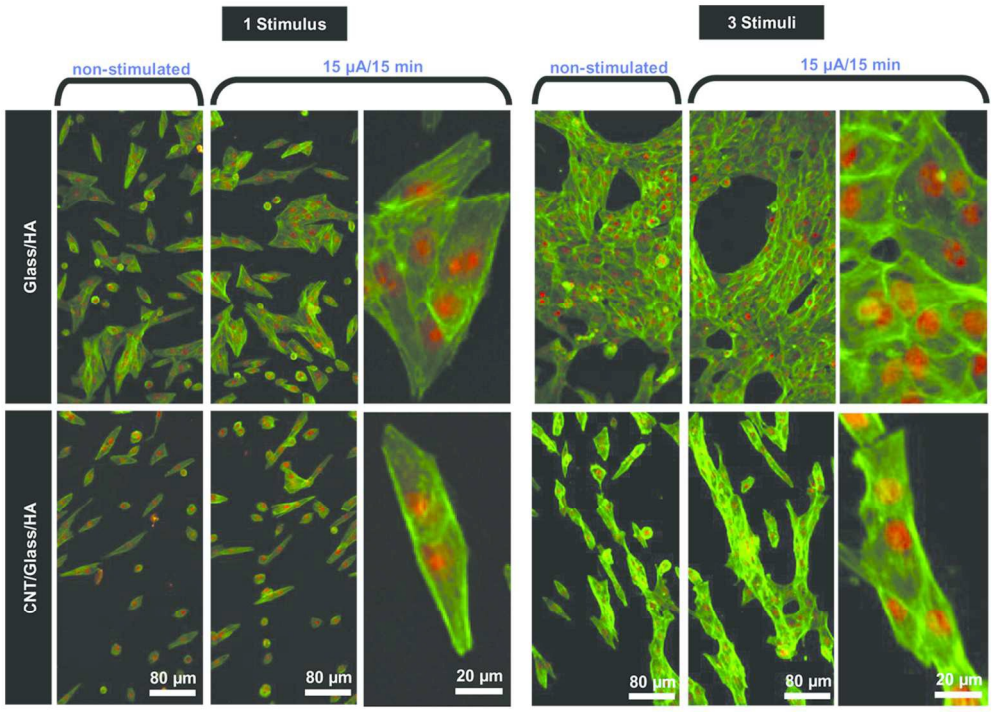

129x93mm (300 x 300 DPI)

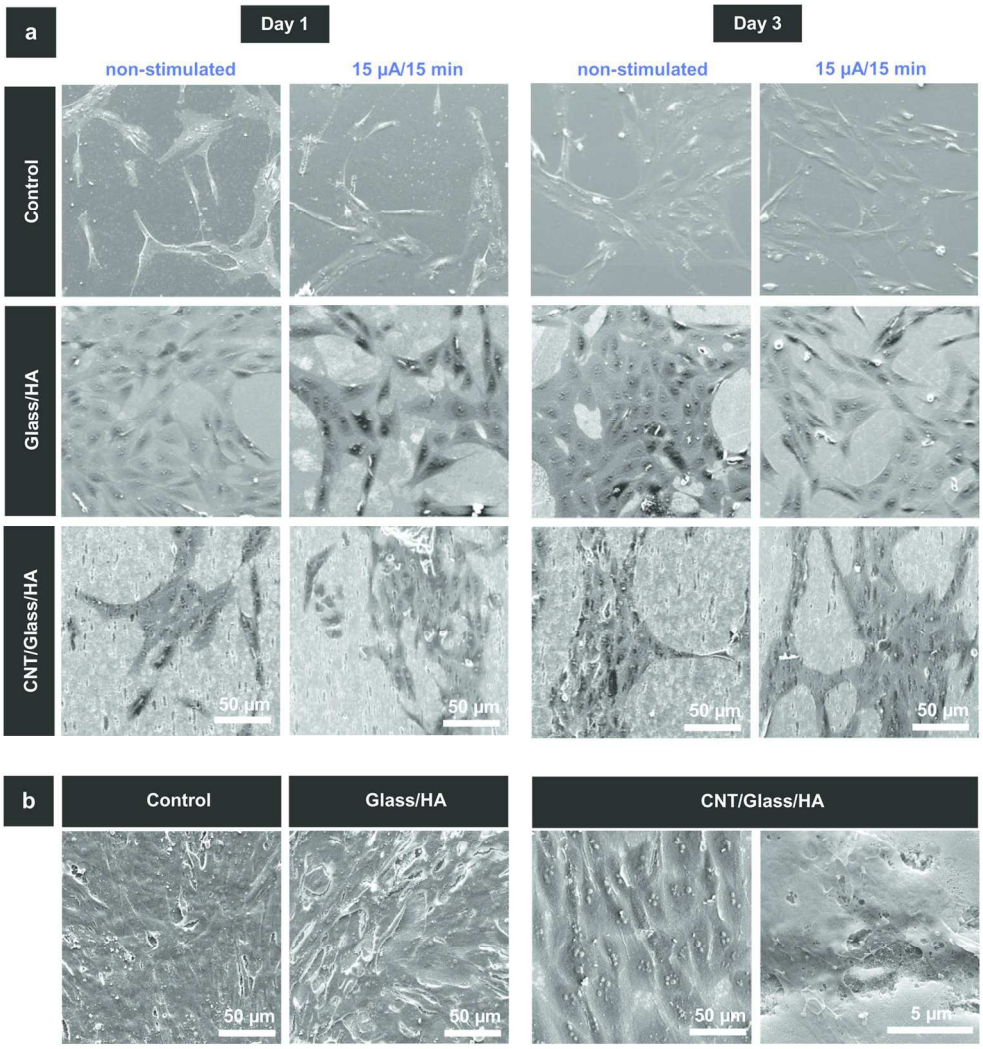

150x157mm (300 x 300 DPI)

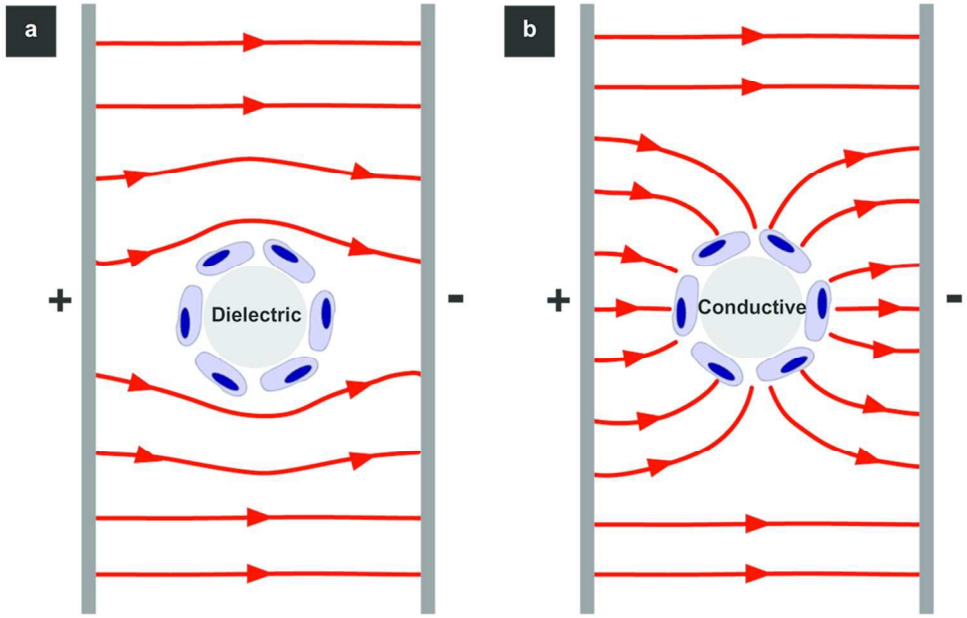

109x71mm (300 x 300 DPI)

Stimulation conditions		Resistor, R1 (kΩ)	Peak-to-peak voltage (V)	Electrical field ($mV.cm^{-1}$)	$Current_{total}$ (μA)	$Current_{samples}$ (μA)	$Current\ density_{samples}$ ($\mu A.cm^{-2}$)
5μA	15 min	3.3	2.7	5.6	100	5±2	65±25
	30 min						
15μA	15 min	1.5	4	15.3	200	15±3	185±30
	30 min						

173x25mm (300 x 300 DPI)

Gene	Forward primer	Reverse primer
GAPDH	CAGGACCAGGTTCACCAACAAGT	GTGGCAGTGATGGCATGGACTGT
Runx2	CAGTTCCCAAGCATTTCATCC	TCAATATGGTCGCCAAACAG
COL1	TCCGGCTCCTGCTCCTCTTA	ACCAGCAGGACCAGCATCTC
ALP	ACGTGGCTAAGAATGTCATC	CTGGTAGGCGATGTCCTTA
OC	CACTCCTCGCCCTATTG	CCCACAGATTCCTCTTCT
OPG	AAGGAGCTGCAGTAGGTCAA	CTGCTCGAAGGTGAGGTTAG

131x33mm (300 x 300 DPI)

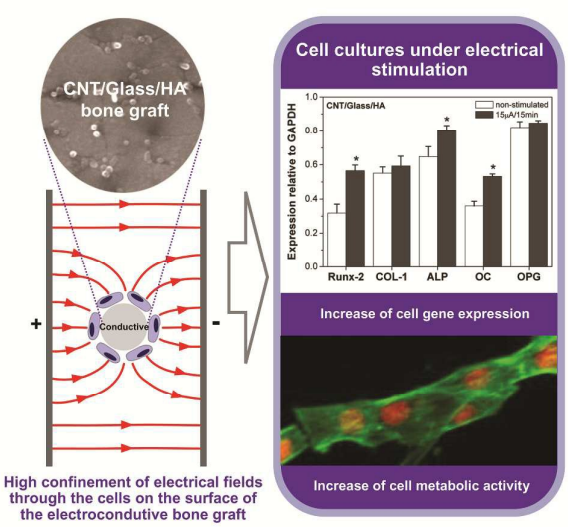

Cell functionalities were controlled *in situ* by an efficient mechanism of delivering electrical stimuli involving conductive biomaterials and non-invasive techniques